Comparison of Semi-Empirical Noise Models with Flyover Measurements of Operating Aircraft

Vieira, A.E.; von den Hoff, B.; Snellen, M.; Simons, D.G.

DOI
10.2514/1.C036387

Publication date
2022

Document Version
Final published version

Published in
Journal of Aircraft

Citation (APA)
Vieira, A. E., von den Hoff, B., Snellen, M., & Simons, D. G. (2022). Comparison of Semi-Empirical Noise Models with Flyover Measurements of Operating Aircraft. *Journal of Aircraft*, *59*(6), 1574-1587. https://doi.org/10.2514/1.C036387

JOURNAL OF AIRCRAFT
Vol. 59, No. 6, November–December 2022

Comparison of Semi-Empirical Noise Models with Flyover Measurements of Operating Aircraft

Ana Vieira,* Bieke von den Hoff,† Mirjam Snellen,‡ and Dick G. Simons§
Delft University of Technology, 2629 HS Delft, The Netherlands

https://doi.org/10.2514/1.C036387

The contribution of the engine and the airframe to the total noise generated by an aircraft varies with the operating conditions. Semi-empirical models are able to account for such variations but require detailed engine and airframe data as input that is not readily available for most aircraft types and operations. This hinders the validation of these models through comparison between predictions and experimental data. This work investigates the sensitivity of semi-empirical models of engine and airframe noise to slight variations of the input data, representative of uncertainties in geometrical parameters and variability of the aircraft operating conditions during flyovers. In addition, the predictions are compared to measurements of A320, A330, and B777 landings and departures. This, together with the sensitivity analysis, indicates frequency regions where a mismatch between measurements and predictions exists. The deviation between predictions and measurements for landings can be partially explained by the underestimation of the sound pressure level of the higher harmonics of the fan. For takeoff, the models predict lower levels than measured. This is hypothesized to be associated with jet-installation noise, which is not accounted for in the semi-empirical models. The predicted spectra of the Airbus A320 and A330 were adjusted to account for jet installation noise, using levels available in the literature. This resulted in a better agreement between modeled and measured spectra at low frequencies.

Nomenclature

A	=	area, m^2
A_n	=	fan nozzle area, m^2
$\mathcal{B}$	=	empirical term of Heidmann's mode
c	=	speed of sound, m/s
D_f	=	far-field directivity patter, dB
d_j	=	characteristic diameter, m
F	=	spectral function of airframe component i
F_1	=	function dependent on the tip Mach number in Heidmann's model
F_2	=	function dependent on the rotor stator spacing in Heidmann's model
F_3	=	directivity correction used to calculate fan noise in Heidmann's model
F_4	=	spectrum shape used to calculate fan noise in Heidmann's model
F_f	=	spectrum falloff for combustor noise
f	=	frequency, Hz
H	=	aircraft altitude, m
k_c	=	convection coefficient
L_c	=	characteristic length, m
l_{strut}	=	length of the strut of the landing gear, m
M	=	Mach number
M_t	=	fan tip Mach number
$\dot{m}_f$	=	mass flow rate across the fan, kg/s
N	=	velocity power coefficient
N_B	=	number of fan blades
N_V	=	number of stator vanes
N_1	=	rotational speed of the fan, %
n_c	=	constant used in Stone's model
n_{slots}	=	number of slots
n_{wheels}	=	number of the wheels of the landing gear
OPWL	=	overall power level, dB
OSPL	=	overall sound pressure level, dB
p_i	=	acoustic pressure, Pa
R	=	distance between the source and observer positions
RSS	=	rotor-stator spacing, %
SPL	=	sound pressure level, dB
S_t	=	Strouhal number
T_j	=	stagnation temperature, K
V_{mix}	=	flow velocity of the jet region, m/s
v_e	=	effective velocity, m/s
α_s	=	empirical scaling coefficient
ΔT_f	=	temperature rise across the fan, K
δ_{co}	=	cutoff correction
θ	=	polar angle, °
θ_{flap}	=	flap deflection angle, °
$\bar{\theta}$	=	angle between the engine inlet symmetry axis and the observer, °
ρ	=	mass density, kg/m^3
ϕ	=	diameter, m

Subscripts

d	=	engine design point
h	=	horizontal tail
ISA	=	International Standard Atmosphere
i	=	airframe component
v	=	vertical tail
w	=	wing
0	=	ambient conditions
3	=	value at the inlet of the combustor
4	=	value at the exit of the combustor
8	=	value at the exit of the turbine

Received 24 January 2021; revision received 2 May 2022; accepted for publication 9 May 2022; published online 2 June 2022.

*Ph.D. Candidate, Aircraft Noise and Climate Effects Section, Faculty of Aerospace Engineering; a.e.alvesvieira@tudelft.nl.
†Ph.D. Candidate, Aircraft Noise and Climate Effects Section, Faculty of Aerospace Engineering; b.vondenhoff@tudelft.nl.
‡Full Professor, Aircraft Noise and Climate Effects Section, Faculty of Aerospace Engineering; m.snellen@tudelft.nl.
§Full Professor, Aircraft Noise and Climate Effects Section, Faculty of Aerospace Engineering; d.g.simons@tudelft.nl.

I. Introduction

THE total noise emitted by an aircraft is the result of different noise sources, which are divided into two main categories: airframe and engine noise. As the name indicates, engine noise originates from the propulsion system and airframe noise is generated

by the interaction between an unsteady turbulent flow and airframe components such as the landing gear, fuselage, and high-lift devices.

The spectral characteristics of aircraft noise depend on the component (e.g., fan, jet, flaps); i.e., the high- and low-frequency content varies for the different aircraft components. Also the sound directivity varies for different components. In addition, the engines and airframe contribution to total noise varies with the aircraft operating conditions [1]. The noise emission of conventional turbofan aircraft during takeoff is generally dominated by engine noise, but for landing, the contribution of airframe and engine noise is approximately equivalent [2]. The landing gear is the most relevant source of airframe noise during landing [3], and the fan dominates engine noise in this flight phase. In addition to the individual noise components, installation and interaction effects also contribute to total noise. Reflection of jet noise on the wing surface [4] and shielding of engine noise by the airframe [5] are examples of installation effects. Noise reflection of engines located under the wings can significantly contribute to an increase of total noise on the ground, whereas the noise generated by rear-mounted engines can be partially shielded by the airframe, resulting in a decrease of total noise [4–6].

Reducing aircraft noise is a complex task, requiring an in-depth knowledge of the different components. Some noise sources, such as the jet and flaps, are well understood by the scientific community but others; e.g., the spoilers and speed brakes, are still far from being fully addressed [2]. Aircraft noise can be assessed by different approaches, depending on the required level of accuracy. Best-practice methods use experimental data to estimate the noise impact on ground. Examples are the methods based on the noise-power-distance (NPD) tables, which use noise certification data to calculate the noise levels on the ground, according to the weight class and flight profile of the aircraft [7]. Another example is FLULA [8], a tool developed by the Swiss Federal Laboratories for Materials Testing and Research (EMPA). This model is based on noise measurements of commercial and military aircraft flyovers and derived individual directivity patters per aircraft type from the measurements. In combination with a flight path and the topography, it predicts noise levels for certain receiver positions [9]. Despite the practicality of best-practice methods in estimating noise contours around airports, they do not provide information about the individual noise components. In contrast, high-fidelity methods and physics-based models provide this information, but require very detailed input data and are computationally expensive, and therefore unpractical for aircraft conceptual design within a multidisciplinary framework [10].

Parametric semi-empirical models are another approach to calculate aircraft noise. These methods determine the noise generated by the different components separately, based both on experimental data and approximations of physics-based models. This approach is therefore more accurate and flexible than best-practice methods and, on the other hand, less complex to implement and less computationally expensive than high-fidelity and physics-based methods. Well-known examples of tools using semi-empirical models are NASA's ANOPP [11–13] and DLR's PANAM [14,15].

This work uses semi-empirical methods to predict aircraft noise. The most relevant airframe noise components (main and nose landing gear, wings, vertical and horizontal stabilizers, slats, and flaps) are calculated with Fink's approach. Jet noise is determined using Stone's model and fan noise with Heidmann's model. In addition, combustion noise is also estimated using the same approach as ANOPP [16,17].

The calculation of airframe noise requires detailed information about the aircraft dimensions, e.g., the wing span, the tire diameters of the main and nose landing gear, and the flap area. This information is relatively easy to obtain. Engine noise predictions require input data such as the jet velocity, fan rotational speed, and values of mass flow rate, temperature, and pressure across the different engine stages. These parameters need to be determined for a specific aircraft operating condition. Typically, programs such as the Gas Turbine Simulation Program (GSP) [18] (the software adopted in this work) are used to obtain the input data required for the engine noise predictions. GSP was developed by the Netherlands Aerospace Centre (NLR) and TU Delft and calculates the gas turbine performance for a reference design point, steady off-design, and transient simulations. It requires a complete modeling of the turbofan stages. This input is hardly available, thus making the comparison of flyover measurements with predictions for different aircraft types a tedious process. However, in comparison with CAA analyses, this method provides faster results with less detailed input data.

This work investigates the sensitivity of engine and airframe noise semi-empirical models to slight variations of the input data. This assessment determines which input influences predictions the most, and which parameters can be approximated without interfering with the final results. For example, for landing aircraft, flyovers measured at the same location show small variations of the flight velocity and rotational speed of the fan. Such variations of the operating conditions influence the engine data input. It is important to know beforehand how such slight variations of the operating conditions influence the predictions.

The findings obtained in the sensitivity analysis are used in the comparison between predicted and experimental values of aircraft noise during landing and takeoff for three different aircraft (Airbus A320, Airbus A330, and Boeing B777). The comparison is made in terms of overall sound pressure level (OSPL) and the spectra obtained at the overhead time.

The semi-empirical methods used in this work are described in Sec. II, and a description of the setup used to measure the aircraft flyovers is given in Sec. III. Section IV.A describes the sensitivity analysis, Sec. IV.B compares predictions with measurements of aircraft noise, and Sec. IV.C analyzes the hypothesis that the discrepancy between the experimental and predicted spectra at low frequencies is due to jet installation noise. Finally, Sec. V summarizes the main results and conclusions of this work.

II. Semi-Empirical Noise Models

A. Engine Noise

Most commercial aircraft are equipped with turbofan engines due to their high thrust-to-weight ratio and fuel efficiency. The engine noise model used in this work includes fan, jet, and combustion noise. The three noise components are determined separately using the models described below.

1. Fan Noise

The fan is the first stage of a turbofan engine and the most important source of engine noise, due to the strong presence of fan noise both during landing and takeoff. Fan noise presents tonal and broadband components. Heidmann's model predicts the free-field noise from the fan, taking into consideration five noise mechanisms: discrete tones from the inlet and exhaust, broadband noise from the inlet and exhaust, and combined tones from the inlet (buzz-saw noise).

Heidmann's model predicts the noise level, spectrum shape, and directivity of the five fan noise components mentioned above. The sound pressure level (SPL) in 1/3-octave bands at a 1-m-radius sphere located at the noise source for each of the five noise mechanisms is given by

$$\mathrm{SPL}(\theta, f) = L_b + F_1(M_t) + F_2(RSS) + F_3(\theta) + F_4(f) \quad (1)$$

The functions $F_{1,2,3,4}$ can be found in [19]. Function F_1 depends on the tip Mach number M_t, F_2 takes into account the rotor-stator spacing (RSS), F_3 contains a directivity correction for the polar emission angle θ (in this model fan noise does not vary with the azimuthal direction), and F_4 represents the spectrum shape, i.e., dependency on the frequency f. The value RSS is given in percentage, relative to the chord of the fan blades. The variable L_b is calculated using the expression

$$L_b = 20\log_{10}\left(\frac{\Delta T_f}{\Delta T_{\mathrm{ref}}}\right) + 10\log_{10}\left(\frac{\dot{m}_f}{\dot{m}_{\mathrm{ref}}}\right) \quad (2)$$

where $\dot{m}_f$ and ΔT_f are the mass flow rate and the temperature rise across the fan, respectively. The variables $\dot{m}_{\mathrm{ref}}$ and ΔT_{ref} are empirical reference values.

The attenuation of the tones in the fan duct is taken into account by the introduction of a tone cutoff correction (δ_{co}) based on the studies of Tyler and Sofrin [20], given by

$$\delta_{\text{co}} = \frac{M_t}{|1 - (N_V/N_B)|} \tag{3}$$

where N_V is the number of stator vanes behind the fan and N_B the number of fan blades.

An empirical correction is used to account for the lining treatment at the inlet and the exhaust [21]. Acoustic lining is a treatment of the engine duct, which allows the attenuation of sound at specific frequencies due to perforations that act as Helmholtz resonators.

2. Jet Noise

This work uses Stone's model, which determines mixing noise and shock-induced noise produced by the jet. Mixing noise is generated by high-velocity jets mixing with the ambient air, and also due to the interaction of the jet exiting the primary and secondary nozzles. Mixing noise has a broadband nature that peaks at low frequencies, around 100–200 Hz.

The method includes the effect of forward flight and of chevrons, and defines three mixing zones. There are two shear layers, one at the bypass airflow and one at the core airflow mixing with the ambient flow. Another mixing zone is generated by the mixing between the bypass and core airflow. These induce sound waves due to the difference of flow velocity. Shock noise is not taken into account in this work because the aircraft analyzed do not operate supersonic.

The unrefracted OSPL of each jet mixing noise source is given by the expression

$$\begin{aligned}\text{UOSPL} = {} & A_s + 10\log_{10}\left[\left(\frac{\rho_0}{\rho_{\text{ISA}}}\right)^2\left(\frac{c_0}{c_{\text{ISA}}}\right)^4\right] + 10\log_{10}\left(\frac{A_n}{|\boldsymbol{R}|^2}\right) \\ & + 10\zeta\log_{10}\left(\frac{\rho_e}{\rho_0}\right) + 10\log_{10}\left[\frac{(v_e/c_0)^N}{1 + \mathcal{B}(v_e/c_0)^{N-3}}\right] \\ & - 5k_c\log_{10}[(1 + M_c\cos\theta)^2 + (\alpha_s M_c)^2]\end{aligned} \tag{4}$$

Here UOSPL is the unrefracted OSPL of the jet mixing component, and the variables c_{ISA} and ρ_{ISA} are the speed of sound and the air density at standard conditions, respectively. The variable $\boldsymbol{R}$ stands for the distance between the noise source and the observer. The speed of sound and air density at ambient conditions are given by c_0 and ρ_0, respectively. The variable A_n is the nozzle area, k_c is the convection coefficient, α_s is an empirical scaling coefficient, and $\mathcal{B}$ is a dimensionless empirical term. The variable A_s is a scaling coefficient that depends on the region of the jet, ζ is a nondimensional value that depends on the outflow velocity, and ρ_e is the mass density in a region of the jet. N is the velocity power coefficient, which is 8 for large mixing noise and 7.5 for other regions of the jet. The values of the constants can be found in [22]. The effective velocity v_e is calculated as follows:

$$v_e = V_{\text{mix}}\sqrt{1 - M\left(\frac{c_0}{V_{\text{mix}}}\right)} \tag{5}$$

where V_{mix} is the flow velocity of the jet region. The convective Mach number of Eq. (4) (M_c) is calculated using

$$M_c = n_c\left[\left(\frac{V_{\text{mix}}}{c_0}\right) - M\right] \tag{6}$$

where n_c is a constant that depends on the region of the jet (large, small, or transitional turbulence) and is determined based on the inner and outer jet velocity and on the engine having a single or dual nozzle. The quantities ρ_e and V_{mix} also depend on the region of the jet, and are determined based on the inner and outer jet temperature, velocity, and mass flow rate. Similarly to the variable n_c, the value of V_{mix} changes for a single- or dual-nozzle engine. Expressions for these quantities can be found in [22].

The sound pressure level can be obtained at a distant point using look-up tables [23] dependent on the UOSPL and the Strouhal number S_t:

$$S_t = \frac{f d_j}{v_e}\left(\frac{T_j}{T_0}\right)^{0.4+(1+\cos\bar{\theta})} \tag{7}$$

where d_j is the characteristic diameter, T_j is the stagnation temperature in the jet region, and $\bar{\theta}$ is the angle between the engine inlet symmetry axis and the observer.

3. Combustor Noise

Combustion noise became more important over the last decades as jet noise has been reduced and they originate in a similar frequency range. Combustion noise has a broadband nature and can be classified as direct and indirect. Direct combustion noise occurs due to the effect of the expansion of the gas mixture on the surrounding gas, producing sound waves. Indirect combustion noise is generated by the convection of nonuniformities through the pressure gradients in the turbine, and consequently creating entropy fluctuations that generate acoustic waves.

The general formulation of the method used to calculate combustion noise in this work [17] is given by

$$\begin{aligned}\text{OPWL} = {} & 10\log_{10}\left(\frac{\dot{m}_3 c_0^2}{\Pi_{\text{ref}}}\right) \\ & + 10\log_{10}\left\{\left(\frac{T_4 - T_3}{T_3}\right)^2\left(\frac{p_3}{p_0}\right)^2\left[\frac{(T_4 - T_8)_d}{T_0}\right]^{-4}\right\} - 60.5\end{aligned} \tag{8}$$

where OPWL is the overall power level, $\dot{m}_3$ is the combustor mass flow rate, Π_{ref} is the reference power of $10^{-12}W$, $(T_4 - T_3)$ is the total temperature rise in the combustor, p_3 is the combustor inlet total pressure, and $(T_4 - T_8)_d$ is the engine design point total temperature extraction by the turbines. When this parameter is unavailable, the value at takeoff can be used instead.

The sound pressure level (SPL) is calculated by applying the spectrum falloff for combustor noise $F_{f,\text{comb}}$, which peaks at 400 Hz (values listed in the literature for 1/3-octave bands), followed by a far-field directivity correction $D_{f,\text{comb}}$, also listed in the literature [17]. This results in the following expression:

$$\begin{aligned}\text{SPL}_{\text{comb}}(f,\theta) = {} & \text{OPWL} + F_{f,\text{comb}} + D_{f,\text{comb}} \\ & + 10\log_{10}\left(\frac{\Pi_{\text{ref}}\rho_0 c_0}{4\pi p_{\text{ref}}^2}\right)\end{aligned} \tag{9}$$

for a distance from the noise source to the observer of 1 m.

B. Airframe Noise

This work uses Fink's model to determine different components of airframe noise: clean wing and tail configurations, flap trailing edge noise, slat leading-edge noise, and main and nose landing gear noise (MLG and NLG, respectively). The noise in the far field of each airframe component i in 1/3-octave bands is calculated using

$$p_i^2 = \frac{\Pi_i F_i(S_t) D_{f,i}(\theta,\phi)}{4\pi|R|^2(1 - M_0\cos\theta)^4}\rho_0 c_0 \tag{10}$$

where D_f is the directivity function and F_i is the spectral function, which depends on the Strouhal number S_t:

$$S_t = (1 - M_0\cos\theta)\frac{f L_c}{M_0 c_0} \tag{11}$$

Here L_c is the characteristic dimension of the airframe component. The variable Π_i is the acoustic power, given by

Table 1 Input data required for the airframe noise predictions

$A_{w,h,v}$	Area of the wing and horizontal and vertical tail, m^2
$b_{w,h,v}$	Span of the wing and horizontal and vertical tail, m
n_{slot}	Number of flap slots
n_{bogies}	Number of bogies
$A_{\text{flap,slat}}$	Flap area, m^2
$b_{\text{flap,slat}}$	Flap span, m
$l_{\text{strut,MLG,NLG}}$	Length of the strut of the MLG and NLG, m
$n_{\text{wheels,MLG,NLG}}$	Number of wheels in the MLG and NLG
$\phi_{\text{MLG,NLG}}$	Diameter of wheels in the MLG and NLG, m
$\Theta_{\text{flap,slat}}$	Flap deflection, rad

$$\Pi_i = K_i(M_0)^{a_i} G_i \rho_0 c_0^3 b_w^2 \tag{12}$$

where K_i is an empirical constant, a_i is a power coefficient relating the acoustic power to the flow speed, b_w is the span, and G_i takes into account the effect of the airframe component and thus differs depending on the component.

The empirical constants, geometrical parameters, and directivity function depend on the airframe noise component and can be found in [24,25]. Table 1 summarizes the geometrical parameters required to calculate airframe noise by Fink's model.

III. Experimental Setup

The flyover measurements were recorded as part of an extensive campaign at Amsterdam Airport Schiphol on three separate days in the Summer of 2019. The microphones were set up outside the airport, at a distance of 670 m from the runway. In Fig. 1 the location of the microphones is indicated by the red cross. On the measurement days a total of 306 aircraft fly-overs were recorded at this location, of which 86 are landings and 238 are takeoffs. Previous research shows that different weather conditions create a maximum level variability of 2 dB [26]. However, the weather conditions were kept as close as possible to the International Civil Aviation Organization (ICAO) atmospheric conditions for noise certification [27]. See Table 2 for the weather conditions. The meteorological data were provided by the Royal Netherlands Meteorological Institute.

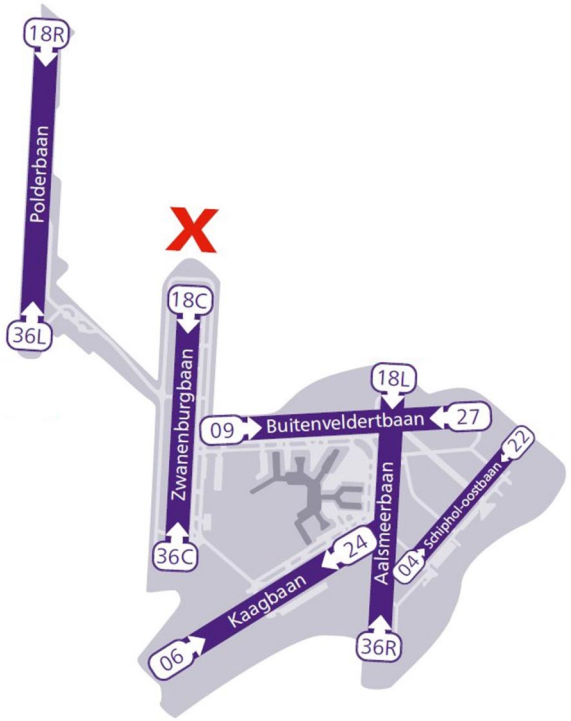

Fig. 1 Measurement location at Amsterdam Airport Schiphol (red cross).

The measurement system, shown in Fig. 2, is an acoustic array of 64 microphones distributed in an Underbrink spiral configuration [28], which was developed and has been used in previous research by Delft University of Technology [29]. The Underbrink configuration is used as it performs well over a broad range of frequencies when considering the maximum side lobe level and array resolution [30]. The microphones can be used collectively to localize noise sources through beamforming techniques. However, for the research presented in this paper the data set is only used for noise spectra and not for source identification.

The array has the dimensions of 4 m × 4 m, and its structure is covered with acoustic absorbing foam to minimize sound reflections. The foam selected was Flamex GU with 15 mm thickness due to its high absorption coefficient. All the microphones were covered with wind shields and were calibrated with a piston phone. The foam used for the wind shields might attenuate the aircraft noise slightly; however, it significantly reduces the interference effects from the wind over the array. It is possible that a single frequency is specifically attenuated due to the nature of the foam.

The microphone (PUI AUDIO 665-POM-2735P-R [31]) signals were sampled at 50 kHz. Also an optical camera was used (Datavision UI-1220LE with a lens Kowa LM4NCL), which had a frame rate of 30 Hz. The camera is placed at the center of the array, and it is used to determine the overhead time. In principal, the aircraft flies straight over the array. A sketch of the flight path of the aircraft with respect to the array is presented in Fig. 3. This figure also includes the polar angle θ and azimuthal angle ϕ. For the research presented in this paper, $\theta = 90°$ and $\phi = 0°$.

The type of aircraft and its height and velocity were determined using an Automatic Dependent Surveillance-Broadcast (ADS-B) receiver. Because not all aircraft have an ADS-B transponder, the aircraft type was also verified with online flight trackers and consecutive frames of the optical camera were used to estimate the height and velocity. The rotational speed of the fan (N_1) was determined based on a de-Dopplerized spectrogram obtained for each flyover [32].

The recorded time-domain pressure data are transferred to the frequency domain with a Fourier transform for which a data block of 0.1 s is used. Before the Fourier transform is applied, the signal is Hanning-weighted and zero-padded with a factor 2. The 0.1 s block size allows for a frequency resolution of 10 Hz.

IV. Results

A. Sensitivity Analysis

This section investigates the sensitivity of the semi-empirical models to slight variations of the input data. These models require a large quantity of input data, which is often not readily available (e.g., inner dimensions of the engines are not provided by the manufacturers) or is estimated with a certain level of uncertainty (e.g., rotational speed of the fan determined for flyover measurements). Therefore, it is important to know beforehand how approximations of the operating conditions and of the airframe and engine geometry influence the predictions. This analysis assesses which input parameters influence predictions the most, and which parameters can be approximated without affecting the final results.

The sensitivity analysis of the semi-empirical models used in this work considers fan, jet, combustion, and airframe noise separately. Takeoff conditions are used to study the influence of the input data on engine noise, because this type of noise is dominant during this flight phase. The sensitivity analysis of airframe noise is made for a landing condition, when the high lift devices and landing gear are deployed. This analysis is based on the A320 aircraft equipped with CFM56 engines. For the landing condition the aircraft flies at an altitude of 50 m and velocity of 65 m/s. The rotational speed of the fan corresponds to $N_1 = 64\%$. The landing gear is deployed, as well as the slats, and the flaps are set at a deflection angle of 30°. For departure, the A320 is flying at an altitude of 400 m at 70 m/s with $N_1 = 84\%$. These operating conditions for takeoff and landing are

Table 2 Weather conditions during the different measurement campaigns

Meteorological condition	ICAO conditions	Day 1	Day 2	Day 3
Date	N.A.	June 22, 2019	July 3, 2019	September 24, 2019
Measurement time start–end (h:m)	N.A.	11:57–17:32	12:01–17:47	11:49–14:30
Operational condition	N.A.	Takeoff	Takeoff	Landing
Location at Schiphol	N.A.	18C	18C	18C
Temperature start to end (°C)	−10 to 35	19.4 to 20.5	17.6 to 19.6	15.9 to 17.1
Humidity start–end (%)	20–75	66–57	45–48	82–81
Pressure start–end (hPa)	N.A.	1023.5–1020.3	1026.5–1026.6	1007.9–1006.8
Wind direction start–end	N.A.	ENE–ENE	N–NNW	SSE–SSE
Wind speed start–end (m/s)	6.3	4–6	4–7	7–7

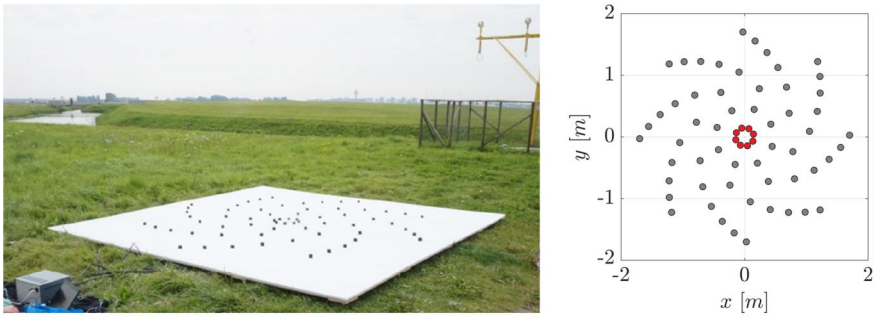

a) Acoustic array **b) Underbrink spiral microphone distribution**

Fig. 2 Acoustic camera used to record the flyovers at Amsterdam Airport Schiphol.

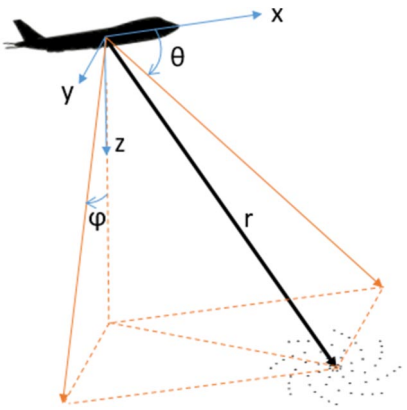

Fig. 3 Polar angle θ and azimuthal angle ϕ with respect to the microphone array.

based on experimental data recorded at Amsterdam Airport Schiphol for this aircraft type (the values used are an average of the recorded operating conditions). The engine performance decks were determined using the GSP [18]. The noise values are calculated for a polar angle of 90° and an azimuthal angle of 0°, i.e., a position below the aircraft with no sideline angle, which corresponds to the aircraft position relative to the array at overhead.

1. Engine Noise

The semi-empirical models used to calculate engine noise depend on the aircraft operating conditions and geometrical parameters. The operating conditions can have a direct influence on noise generation, e.g., the Mach number in the jet noise prediction (see Sec. II.A.2), but can also influence other parameters (e.g., the values of temperature and mass flow across the engine states). Therefore, for clarity, this analysis classifies the input data into three categories:

1) Operating conditions: Mach number (M), aircraft altitude (h) (envelope parameters), and rotational speed of the fan (N_1)

2) Parameters influenced by the operating conditions: e.g., mass flow rate and temperature variation across the engine

3) Geometrical parameters: e.g., wing span and fan diameter

The operating conditions and geometrical parameters were varied 20% relative to the baseline takeoff case of the A320. The parameters influenced by the operating conditions were determined based on a 20% variation of the Mach number, altitude, or rotational speed of the fan; i.e., the influence of the operating conditions on these parameters is evaluated separately.

The sensitivity analyses for the three components of engine noise are performed individually because they are determined with different semi-empirical methods. First, jet noise is analyzed, then the analysis of fan and combustion noise is presented.

a. Jet Noise. Table 3 displays the two categories of input data required for the calculation of jet noise. Given the large number of input variables, only the most relevant plots are displayed in this paper.

The Mach number M was varied 20% relative to the original value, which resulted in an offset of less than 1.5 dB relative to the baseline case over the entire frequency range of the noise spectra (from 50 to 10,000 Hz; see Fig. 4). For this, also the parameters influenced by the Mach number were changed accordingly. The importance of ensuring the right engine parameters is investigated by quantifying the effects of the change in jet velocity, mass flow rate, and temperature separately. It was observed that the change of the inner and outer jet velocity resulting from a 20% variation of the Mach number modified the jet noise spectrum with a maximum deviation of 0.7 dB. However, this was not the case for the variation of the inner and outer mass flow rate and jet temperature, which did not influence the noise spectrum.

The inner and outer jet velocity, mass flow rate, and jet temperature also depend on the aircraft altitude and rotational speed of the fan.

Table 3 Input required for the jet noise prediction

Parameters influenced by the operating condition	Geometric parameters
Inner and outer jet velocity	Inner and outer jet area
Inner and outer mass flow rate	Length between the inner/outer jet exhaust plane
Inner and outer jet temperature	

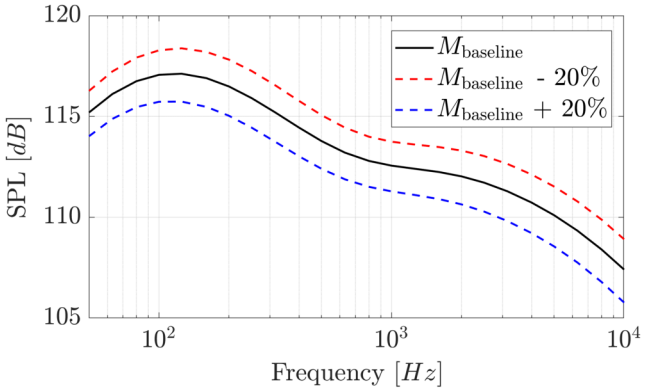

Fig. 4 Variation of jet noise with the aircraft Mach number *M*.

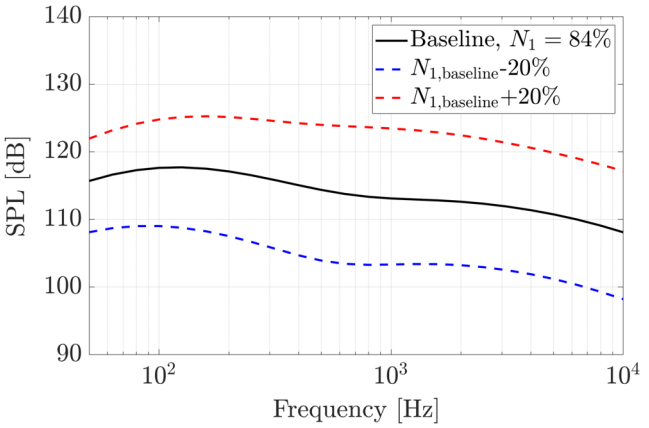

Fig. 5 Variation of jet noise with the rotational speed of the fan, N_1.

A variation of 20% of the aircraft altitude resulted in slight variations of the inner and outer jet velocity, mass flow rate, and jet temperature. Such small variations resulted in an unaltered spectrum of jet noise.

A 20% variation of N_1 did not significantly affect the inner and outer mass flow rate and jet temperature. The inner and outer jet velocity, however, changed significantly with the value of N_1, and consequently the spectrum of jet noise shows differences relative to the baseline case, as shown in Fig. 5. In this case, the SPL difference relative to the baseline case is not constant over the frequency and has a maximum offset of 10.4 dB.

The three geometrical parameters of Table 3 were also varied 20% relative to the values of the CFM56 engine. The variation of the jet areas resulted in an offset of the noise spectrum less than 1 dB relative to the baseline case. The variation of the length between the inner/outer jet exhaust planes did not change the jet noise spectrum. This is not a parameter easily found in the literature, so additionally to the 20% variation, its value was also doubled and reduced by half in relation to the baseline to understand if a rough estimation would have a great impact on jet noise. It was found that such a rough approximation also did not alter the noise spectrum.

Table 4 summarizes the results obtained for the sensitivity analysis of jet noise with the input data. Some parameters are not shown in the table because they did not influence the noise results.

This sensitivity analysis shows that N_1 influences jet noise the most due to the indirect change of the inner and outer jet velocities. When comparing flyover measurements with predictions, an uncertainty of the aircraft velocity and altitude of around 20% is not expected to result in significant deviations in the noise spectrum. The value of N_1, however, should be estimated as accurately as possible.

Table 4 Change of jet noise spectrum relative to the baseline case for a 20% variation of the input data

Parameter	Maximum deviation (absolute value), dB
Mach number	1.3
Rotational speed of the fan	10.4
Inner and outer jet area	0.7

Table 5 Input required for the fan noise prediction

Parameters influenced by the operating conditions	Geometric parameters
Total temperature rise	Fan rotor diameter
Mass flow rate	Number of vanes
	Number of blades
	Rotor-stator spacing
	Fan rotor tip Mach number at design point

b. Fan Noise. The sensitivity study of fan noise was performed in a similar manner as jet noise. Table 5 shows the parameters required for the fan noise prediction, divided into geometric input and parameters influenced by the operating conditions.

The Mach number was reduced and increased with 20% with no variation of fan noise. The changes in the values of the total temperature and mass flow rate across the fan caused by this Mach variation were small, and therefore the noise spectrum remained unaltered. The same was observed for a 20% variation of the aircraft altitude.

A 20% variation of the rotational speed of the fan, as expected, has a significant influence on the fan noise spectrum. This parameter influences the total temperature rise and mass flow rate across the fan, as well as the cutoff correction and the frequency of the blade passing frequency (BPF) and its harmonics.

The difference is not significant in terms of OSPL for an increase of 20%, but the harmonics were moved to different 1/3 octave bands, which can lead to a significant difference in the noise characteristics (e.g., sharpness). Figure 6 shows the importance of an accurate estimation of N_1.

The fan diameter is an important parameter, because it is used to determine the rotor tip Mach number and the cutoff correction. However, no change in the noise spectrum was observed for a change of 20% relative to the baseline value.

The number of blades was changed from the original value of 36 to 30 and 40 (approximately a 20% variation rounded to integer numbers) without resulting in any change in the fan noise prediction, because the frequency is discretized in 1/3-octave bands and the fan BPF and harmonics remain within the same band. The number of fan rotor blades is readily available, and therefore there is no reason for a rough estimate of this parameter. In contrast, the number of vanes is difficult to obtain but also did not influence fan noise for a 20% variation.

Another geometrical input difficult to find in the literature is the rotor-stator spacing, RSS. The fan noise spectrum remained unaltered for a 20% variation relative to the baseline value of 300%. However, because this parameter is difficult to obtain, the deviation from the correct value can be higher than 20%, and therefore other values were also tested. A low value of RSS, equal to 100% (i.e., the space between

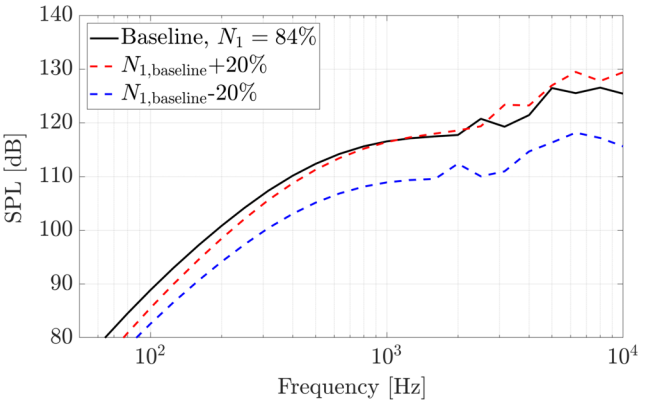

Fig. 6 Variation of fan noise with the rotational speed of the fan, N_1.

Table 6 Change of fan noise spectrum relative to the baseline case for a 20% variation of the input data

Parameter	Maximum deviation (absolute value), dB
Rotational speed of the fan	10
Fan rotor tip Mach number at design point	1

the rotor and the stator is equal to the chord of a fan blade) showed a maximum deviation of 3.5 dB relative to the baseline value. This deviation decreases to 1.5 dB for a value of RSS of 200%, which is still a rough estimate, but closer to the real value.

In addition to the parameters shown above, the fan rotor tip Mach number at the design point, M_{DP}, was varied 20% relatively to the baseline value of 1.43, resulting in a constant offset of approximately 1 dB over the 1/3-octave bands.

This analysis indicates that the operating rotational speed of the fan has the greatest influence on fan noise, as expected, but also that most geometric parameters can be approximated. Small variations of the aircraft velocity and altitude for the same N_1 do not require new predictions.

Table 6 summarizes the results obtained for the sensitivity of the fan noise to the input data.

c. Combustion Noise. The sensitivity study of combustion noise considers the variables shown in Table 7. The operating conditions do not directly influence the values of combustion noise, but affect parameters that are important to determine this type of noise.

The total pressure at the inlet of the combustor, p_3, showed only negligible variations for a 20% variation of the Mach number and altitude, and therefore did not influence combustion noise. However, the parameter p_3 did show some variation with N_1.

Changes of the mass flow rate at the inlet of the combustor ($\dot{m}_3$) for the variation of the operating conditions resulted in an unaltered spectrum of combustion noise. The same was observed for the influence of the operating conditions on the temperature variation across the combustor.

Therefore, N_1 is the only operating condition affecting combustion noise when varied 20% due to the change of the total pressure inlet of the combustor. Figure 7 shows that a 20% overestimation of N_1 will lead to a maximum deviation of 3.3 dB.

The component $[(T_4 - T_8)_d/T_0]^4$ of Eq. (8), also denominated as T_{ref} in this work, has a great influence on combustion noise but does not change with the operating conditions because it should be calculated for the design point of the engine. Additionally it is not a geometric parameter, and therefore it has not been included in Table 7. However, these parameters are often not available, and literature recommends to estimate the value at maximum takeoff conditions. Figure 8 shows that a 20% variation of this term results in a maximum offset of 3.9 dB, and therefore it has to be correctly assessed.

Changing the value of the design tip Mach number within 20% of the real value does not influence the combustion noise spectrum. Table 8 summarizes the results obtained for the sensitivity analysis of the combustion noise with the input data.

Table 7 Input required for the combustion noise prediction

Parameters influenced by the operating conditions	Geometric parameters
Total pressure at the inlet of the combustor	Design tip Mach number
Total temperature at the inlet of the combustor	
Mass flow rate at the inlet of the combustor	
Total temperature at the outlet of the combustor	
Total temperature at the exit of the turbine	

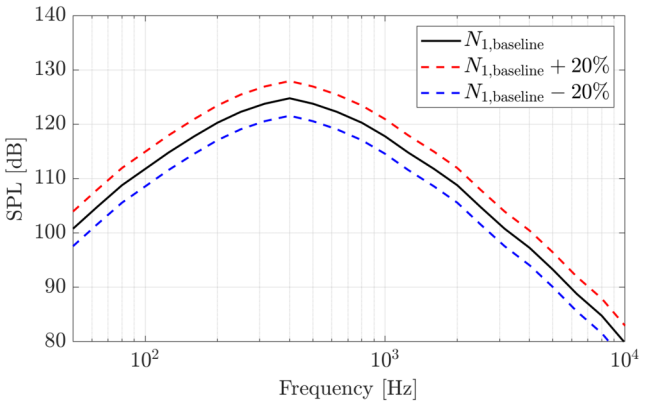

Fig. 7 Variation of combustion noise for different values of N_1.

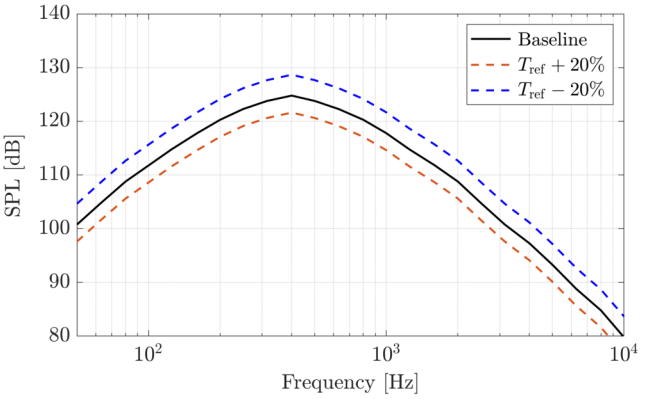

Fig. 8 Variation of combustion noise for different values of T_{ref}.

2. Airframe Noise

The input data required for the airframe noise calculations can be found in Table 1. Figure 9 shows the resulting spectrum from a 20% variation of the Mach number and how important this parameter is for a correct noise prediction.

Flap noise is an important component of airframe noise during approach. It was found that a change of the flap deflection angle from the initial value of 30° to 15° resulted in a maximum variation of −2 dB compared with the baseline case. Therefore, a small difference of the flap deflection is not expected to significantly change airframe noise predictions. This is important for the comparison with flyover measurements because the deflection angle is

Table 8 Change of combustion noise spectrum relative to the baseline case for a 20% variation of the input data

Parameter	Maximum deviation (absolute value), dB
N_1	3.3
T_{ref}	3.9

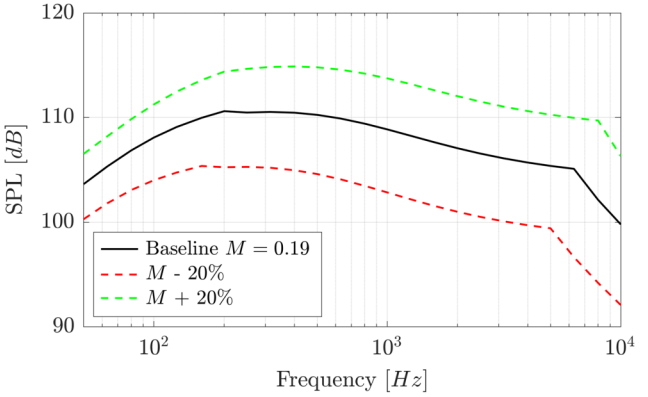

Fig. 9 Variation of airframe noise with the aircraft velocity.

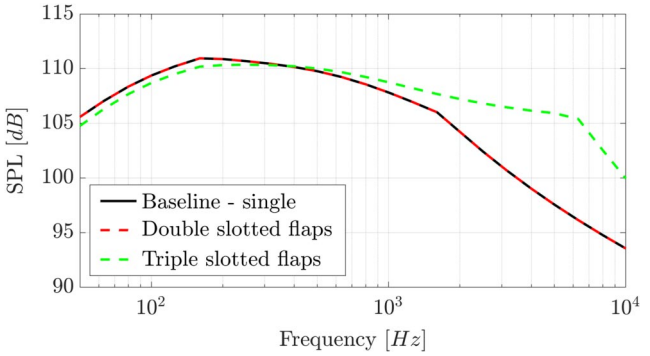

Fig. 10 Variation of airframe noise with the number of flap slots.

not available. For the comparison of prediction with flyover measurements, normally it is necessary to assume a value typical for landing or takeoff.

A 20% variation of the flap area or span did not significantly affect airframe noise, because the difference relative to the baseline case was only noticeable at high frequencies, where fan noise is more important than airframe noise. The number of flap slots, however, has a significant influence on airframe noise (see Fig. 10).

A variation of 20% of the wing span and area only reflected in a lower than 1 dB change of airframe noise. The same was verified for a 20% variation of the horizontal and vertical tail area and span.

Landing gear noise is calculated using the length of the struts and the diameter of the wheels. The number of bogies and wheels can be easily determined, as well as the length of the struts and the diameter of the wheels. A variation of 20% in the length of the strut of the main and nose landing gear did not change the airframe noise spectrum. The 20% variation of the diameter of the wheels of the main landing gear (MLG) resulted in a 0.5 dB offset for the entire frequency range comparatively to the baseline case. A variation of 20% of the wheels diameter of the nose landing gear did not result in a change of airframe noise.

The aircraft Mach number together with the wing area and the flap span have the most impact on airframe noise as summarized in Table 9.

Table 9 Variation of airframe noise relative to the baseline case

Parameter	Maximum deviation (absolute value), dB
Wing area	0.7
Wing span	0.5
Flap area	2
Flap span	4.9
Diameter of the wheels of the MLG	0.5
Mach number	4.8
Flap deflection	1.8

B. Comparison of Semi-Empirical Noise Models with Experimental Data

This section compares measurements of aircraft noise during landing and takeoff with the semi-empirical models described in Sec. II. The comparison is made in terms of total noise. Ideally, the different noise sources would be separated using beamforming and compared with the corresponding prediction. However, although the separation of engine and landing gear noise, e.g., can be done using beamforming techniques [3,31], quantifying the contribution of the high-lift devices or of the wing/fuselage noise remains a challenge, as those noise sources are distributed over a large area.

The aircraft Airbus A320, Airbus A319, Airbus A330, and Boeing B777 were selected for this comparison because of the large data set per type. The noise values are determined at the source location; i.e., the values measured at the acoustic array were propagated back to the aircraft location using spherical spreading and including the atmospheric absorption [33–35]. The A330 is not shown for landing, because no measurements were available. First the variation within a measurement set of an aircraft type is analyzed. Following that, the predictions are compared with the measurements per aircraft, and some comparisons are made between the aircraft types.

The OSPL variation for each aircraft type is presented in Fig. 11.

The variation of OSPL is higher for takeoff than for landing, as expected, because landing aircraft must follow the Instrument Landing System (ILS), which results in regular trajectories. Therefore, all landing aircraft were centered at the acoustic array, whereas some takeoff flyovers were visibly misaligned; i.e., the azimuthal angle was slightly off from 0°. The values of OSPL were obtained for a time interval of 0.1 s and averaged over the 8 microphones at the center of the array (microphone positions in red in Fig. 2b).

The noise spectra in 1/3-octave bands of different flyover measurements of the A320 are shown in Fig. 12, both for landing and takeoff. These plots show the corresponding aircraft velocity and the rotating speed of the fan for each flyover. For landing, the noise spectra of the different flyovers do not show significant variation as the operating conditions are similar. The noise spectra for takeoffs, however, present more variability and significant differences at high frequencies. It was observed that the takeoff flyovers centered at the array (green, light blue, and pink spectra of Fig. 12b) presented more high-frequency content than when misaligned (red and blue spectra).

Figure 13 shows the spectra at overhead time of A320 (gray) and A319 (red) flyovers. The A319 aircraft is powered by CFM56 turbofans, similarly to the A320. In addition, the dimensions of the two aircraft are similar, but the A319 has a shorter fuselage length. Therefore, as expected based on the results of the sensitivity analysis, the spectra of the A319 and A320 aircraft are similar. Thus from here onward, only the A320 will be explored as representative of these two aircraft.

The takeoff noise spectra of the A320 indicate that the low frequencies correspond to higher sound pressure levels than high-frequency noise; i.e., jet and combustion noise are dominant. Such difference is not so evident for the B777 (see Fig. 14). All three aircraft types are equipped with modern turbofan engines with high values of bypass ratio (BPR); therefore, jet noise is not expected to

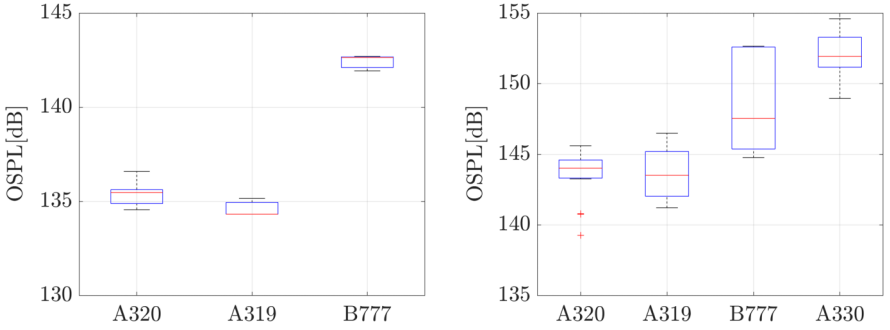

a) Landing **b) Take-off**

Fig. 11 Variation of the measured OSPL at the aircraft location for each aircraft type.

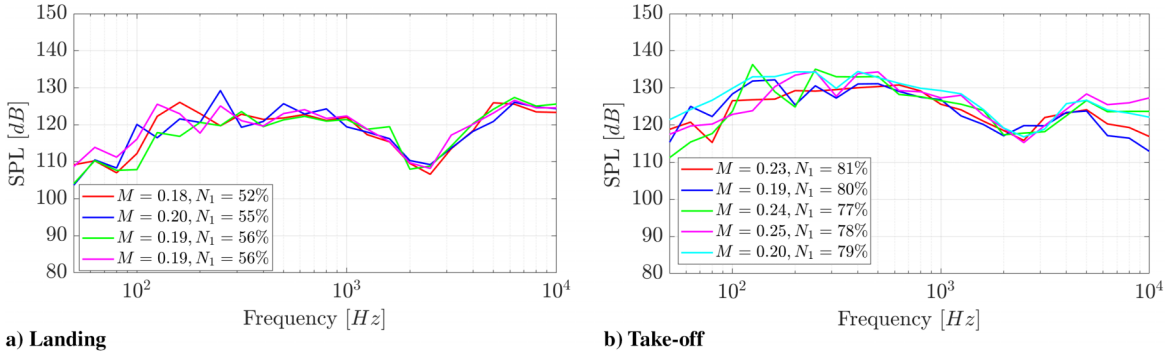

a) Landing **b) Take-off**

Fig. 12 Measured noise spectrum of A320 flyovers.

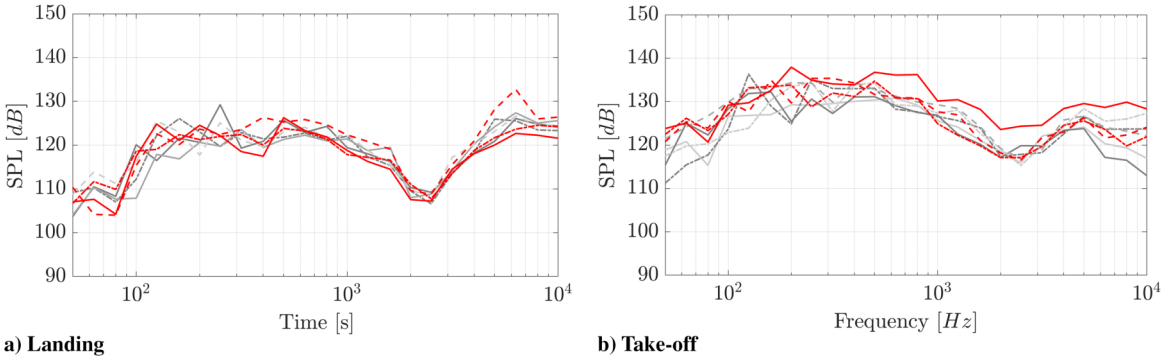

a) Landing **b) Take-off**

Fig. 13 Noise spectra of A320 (in gray) and A319 (in red) aircraft of different flyover measurements.

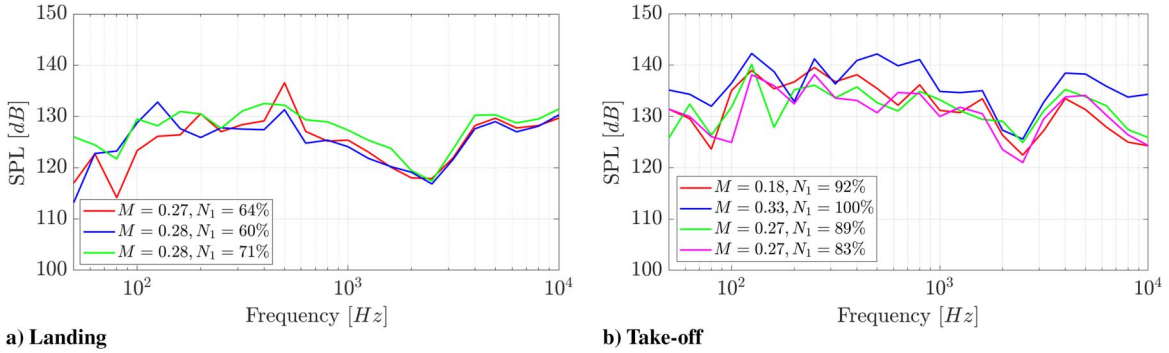

a) Landing **b) Take-off**

Fig. 14 Measured noise spectrum of B777 flyovers.

play a dominant role during takeoff. We will later investigate the cause of this unexpected high level of jet noise of the A320.

The noise spectra for all three landing aircraft show similar values of sound pressure levels for high and low frequencies, slightly higher for values above 3000 Hz. The low sound pressure level values between 1600 and 3150 Hz observed for the A320 seem to indicate the presence of lining treatment of the engine ducts because the CFM56 engine typically has a BPF value in this frequency range.

The measured noise spectrum plots for all aircraft types show a low variability, but the aircraft operating conditions are similar (Mach number and N_1), so the semi-empirical predictions used average values of altitude, N_1, and aircraft velocity. These predictions combined the different noise components at the source position, assuming a unit sphere with a radius of 1 m. The predictions obtained for the three aircraft types are presented separately.

1. *Airbus A320*

The polar plots of Fig. 15 show the OSPL values of the different noise components, predicted for the A320 during landing and takeoff (for an azimuthal angle of 0°). The polar plot for landing A320 (Fig. 15a) shows a negligible contribution of the jet to the total noise. Fan and combustion noise are dominant for polar angles higher than 60°, and airframe noise is predominant for polar angles below 60°.

For takeoff, according to Fig. 15b, fan and combustion noise are dominant for most observer polar positions, but jet noise has an important contribution to the total noise. In addition, airframe noise is negligible compared to other noise sources. The relative importance of the different noise components predicted by the semi-empirical methods is in line with what is theoretically expected: predominance of engine noise for takeoff and a more similar contribution of engine and airframe noise for landing.

Figures 16 and 17 compare the predicted landing and takeoff spectrum of the A320 with results obtained from different measurements, for a receiver at $\theta = 90°$ and $\phi = 0°$, i.e., in agreement with the overhead position of the acoustic array.

The predictions for the landing phase show lower values of SPL than the measurements for the entire frequency range except for frequencies between 2000 and 3150 Hz. The same SPL difference is found for frequencies higher than 3150 Hz, in the spectral region associated with fan noise.

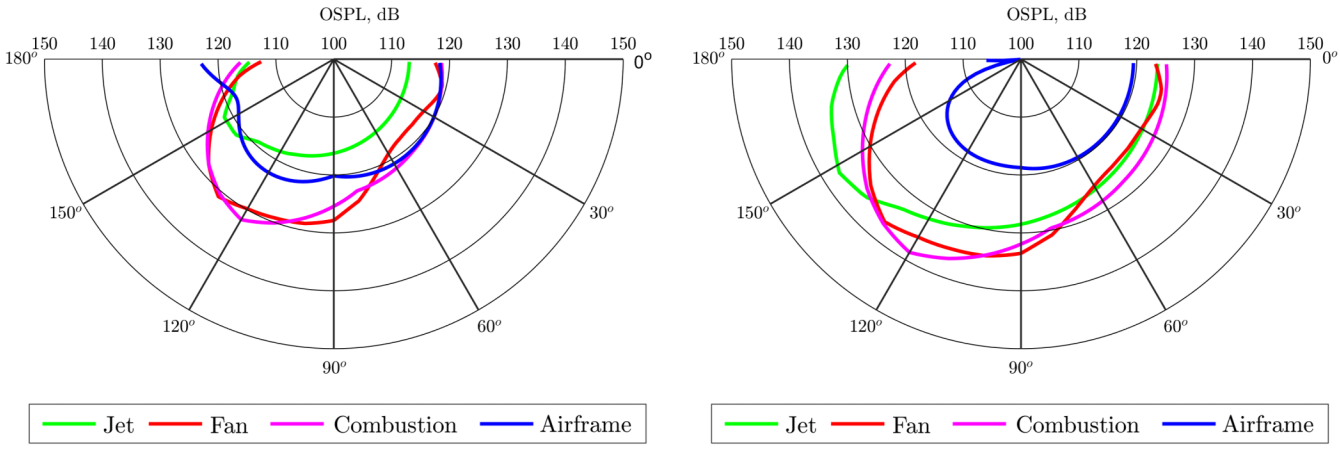

a) Landing **b) Take-off**

Fig. 15 Values of OSPL predicted for the A320 over different polar angles and azimuth angle $\phi = 0°$.

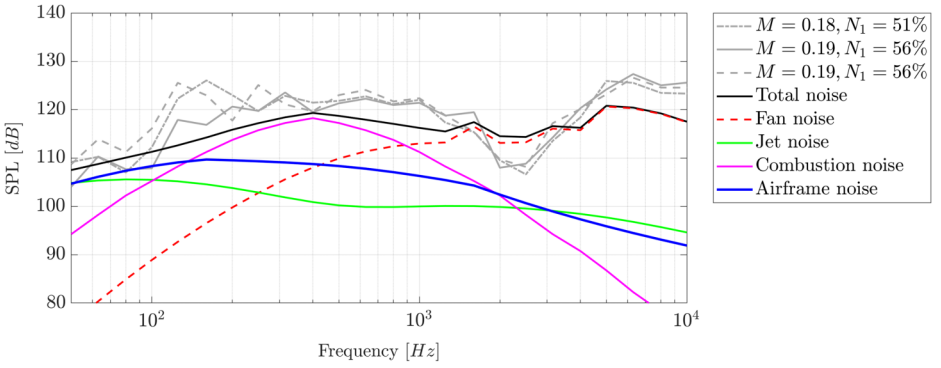

Fig. 16 Comparison of the predicted (in color) and measured (in gray) spectra of the A320 for landing.

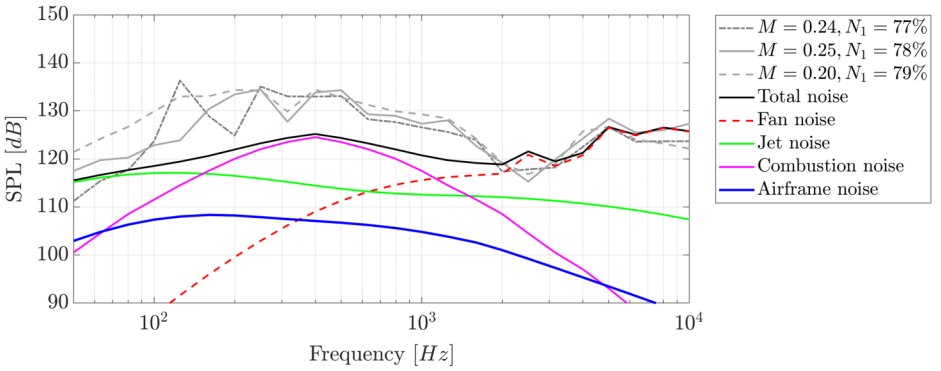

Fig. 17 Comparison of the predicted (in color) and measured (in gray) spectra of the A320 for takeoff.

The comparison between the experimental and predicted noise spectrum of the A320 for takeoff, shown in Fig. 17, shows a good agreement for the high-frequency range, where fan noise is dominant. The liners were approximated using typical values found in the literature [21], which according to Figs. 16 and 17, led to an underestimation of the fan noise suppression in the frequency range 2000–3150 Hz. For the low-frequency range, the noise prediction is approximately 10 dB lower than the measurements.

This discrepancy of SPL at low frequencies between the experimental and predicted noise spectrum is hypothesized to be associated with jet-installation noise (JIN). Recent work used high-fidelity methods to investigate this effect, and it was found that high values of low-frequency noise amplification can occur in the far field [4]. According to this work, this installation effect is more evident for observers at $\theta = 90°$.

2. *Boeing B777*

The OSPL polar plots obtained for the B777, shown in Fig. 18, present some differences compared to the results obtained for the A320, in particular the dominant role of airframe noise for the B777 during landing for all polar angles. The comparison between the predicted and the measured noise spectrum is shown in Figs. 19 and 20 for approach and takeoff, respectively.

The experimental noise spectrum of Fig. 19 shows a good agreement with that predicted for the low-frequency range up to 1600 Hz, but the high frequencies are underestimated, clearly due to low values of fan noise.

For takeoff, Fig. 20 shows that the agreement between the experimental and measured noise spectrum is limited for high frequencies. There is evidence of JIN at the low frequencies, but the offset between the measured and predicted spectra is smaller than for the

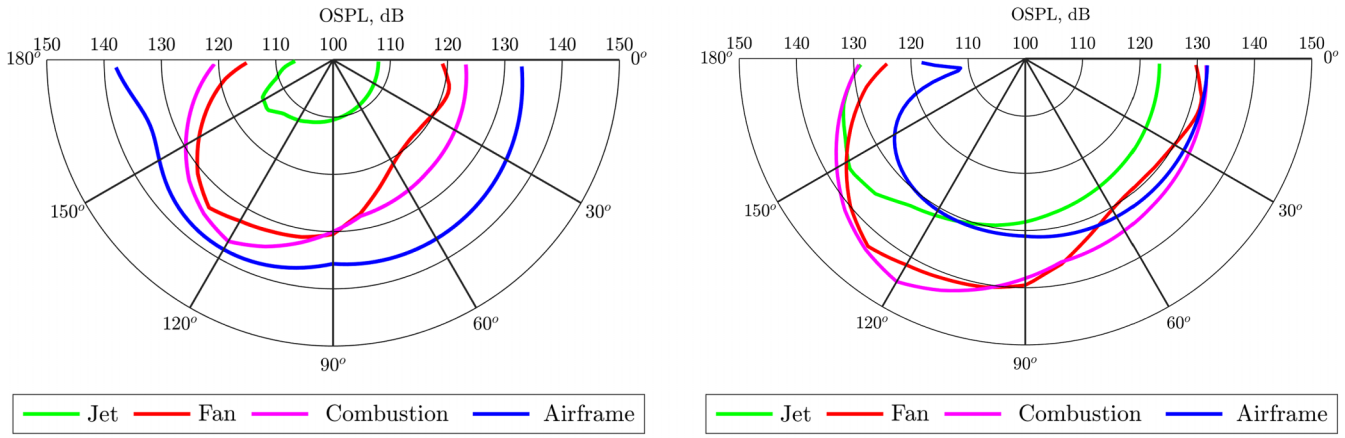

a) Landing **b) Take-off**

Fig. 18 Values of OSPL predicted for the B777 over different polar angles and azimuth angle $\phi = 0°$.

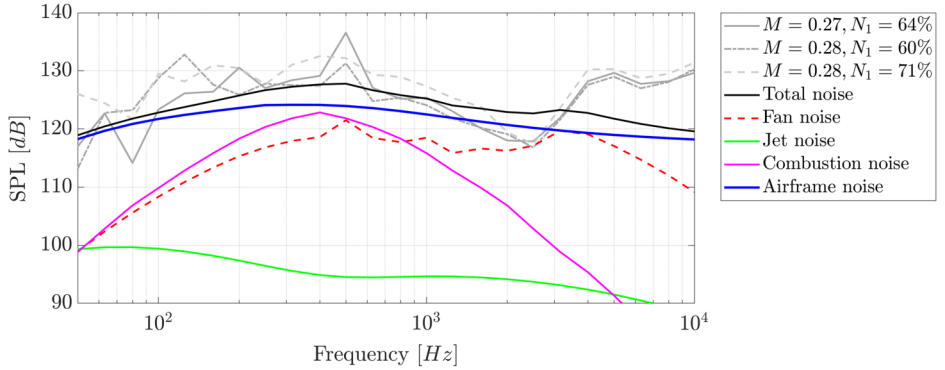

Fig. 19 Comparison of the predicted and measured spectra of the B777 for landing.

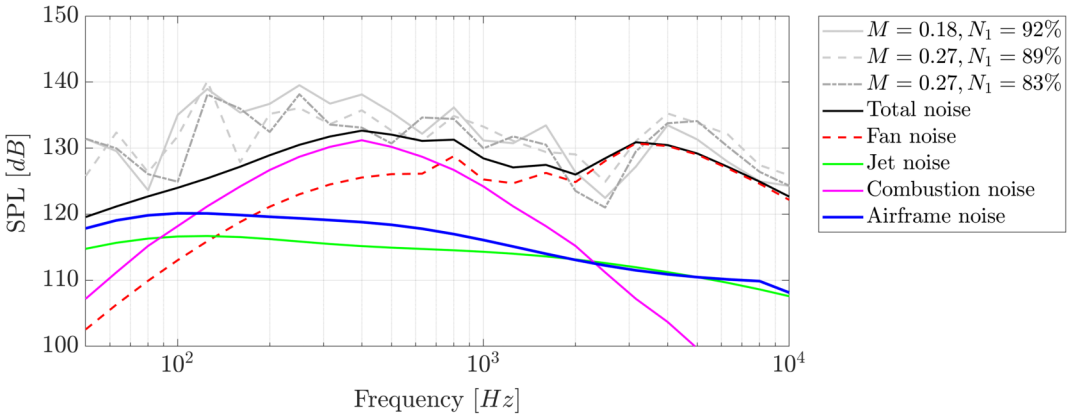

Fig. 20 Comparison of the predicted and measured spectra of the B777 for takeoff.

case of the A320. This is an expected result, because jet noise assumes almost the same importance as fan and combustion noise for the A320 during takeoff, which is not the case for the B777, which presents higher noise contribution of fan and combustion than jet noise.

3. *Airbus A330*

The OSPL polar plot for the A330 during takeoff condition is shown in Fig. 21.

Figure 22 shows the measured and predicted noise spectrum of the A330 for takeoff. The predicted noise spectrum shows a good agreement with the measurements for high frequencies. The low-frequency range shows a significant difference, similar to what was observed for the A320 and B777.

The three aircraft analyzed consistently showed similar SPL deviations between measurements and predictions at a polar angle of 90° and azimuthal angle of 0°. According to the sensitivity analysis of Sec. V.A, these deviations are not related with approximations of the aircraft operating conditions, as the slight variations of the aircraft altitude, velocity, and the rotational speed of the fan observed experimentally are not expected to significantly affect the noise spectrum. Also the low variability observed in the measured noise spectrum of the A320 and B777 indicates that the differences between experiments and predictions are not related with deviations of the operating conditions.

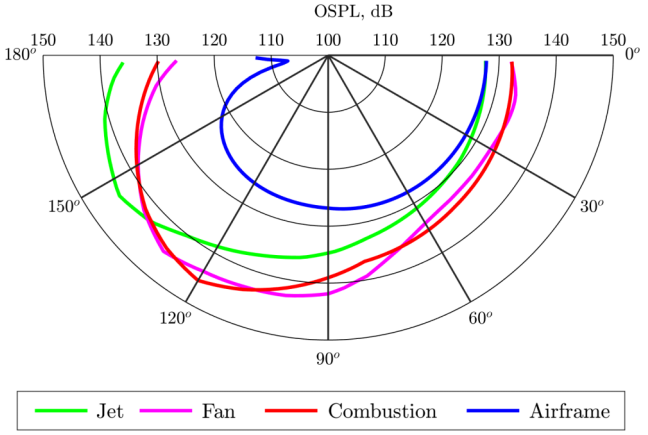

Fig. 21 Values of OSPL predicted for the A330 over different polar angles and azimuth angle $\phi = 0°$ during takeoff.

The predicted and measured noise spectra for takeoff aircraft present a good agreement at high frequencies; i.e., the first harmonics of the fan are accurately predicted. For low frequencies (associated with jet noise for takeoff aircraft), however, the measured and predicted spectra present significant differences. Research on jet installation noise has shown that the SPL at low frequencies can be reinforced up to 14 dB in the far field, due to jet noise reflections on the wing surface [4]. This is expected to result to an increase of OSPL of approximately 5 dB for an observer at a polar position of 90°.

For landing aircraft, the difference between predicted and measured spectra at low frequencies is smaller than what was observed for takeoff. This is in line with the role of jet installation noise as described above, as the values of jet noise are lower for landing than for takeoff, which results in lower values of noise reflection. For high frequencies, the measured and predicted spectra present significant differences for landing for the three aircraft analyzed, indicating that the higher harmonics of the fan are underestimated in the modeling. The case of the B777 supports this hypothesis, as the predicted noise spectrum of the B777 during landing presented the worst agreement with the measurements. This aircraft is equipped with two GE90-115B turbofans, which have 22 fan blades and a maximum rotational speed of 2602 RPM. At full power the BPF is therefore approximately 950 Hz. At takeoff, assuming a typical value of $N_1 = 90\%$, the fifth harmonic is located at the center frequency of 4000 Hz. It is visible that the B777 prediction at this frequency does not match the experimental results as well as the A320 and A330, which have BPF values around 2850 and 1960 Hz, respectively. For landing, assuming a typical value of $N_1 = 60\%$, the BPF of the B777 is 572 Hz, and consequently only harmonics higher than the fifth are located at the high frequencies, and these are clearly underestimated compared with the experimental spectra.

Table 10 shows the measured and predicted OSPL values for the cases analyzed above. The OSPL predictions are closer to the measured values for landing than for takeoff, as observed in the spectra.

Table 10 Predicted and measured OSPL for landing and takeoff

	Airbus A320		Boeing B777		Airbus A330	
OSPL	Landing	Takeoff	Landing	Takeoff	Landing	Takeoff
Predicted	130.6	136.4	138.0	142.5	144.4	–
Measured	135.5	144.0	142.0	148.0	152.9	–
Offset	4.9	7.6	4.0	5.5	8.5	–

C. Jet Installation Noise Correction

To investigate whether including JIN would improve the model, this section adjusts the values of jet noise of the A320 and A330 aircraft during takeoff based on results of jet installation noise obtained with high-fidelity methods. The values used to account for the jet installation noise were based on the work of Rego et al. [4], which uses the lattice Boltzmann method and the Ffowcs-Williams Hawkings analogy to determine the far-field spectra from an isolated and installed jet at different polar angles. These predictions are determined for takeoff aircraft, for different relations between the nozzle exit diameter D_j, length of the plate L (approximating the lower surface of the wing), and the normal distance from the center of the nozzle exit to the plate (radial installation). Experimental research on installing a flat plate around the jet exhaust by Rego et al. [36] confirms that an installed plate amplifies the spectrum for low frequencies and midfrequencies with respect to an isolated jet. Additionally, this research confirms that an increased length of the plate amplifies the installation noise in the low-frequency range. The radial placement of the plate with respect to the jet accounts for amplification of the midfrequency range, where closer to the jet implies an increase in SPL.

The spectra of the isolated and installed jet in the work of Rego et al. [4] are plotted against the Strouhal number St, given by

$$\mathrm{St} = \frac{D_j}{U_j} f \tag{13}$$

in which U_j is the nominal jet velocity.

The values of those plots were used to adjust the spectrum of jet noise obtained with Stone's method. The high-fidelity methods were only applied for takeoff conditions and for a limited number of wing chord dimensions. The relation between the chord section aligned with the engine position for the B777 is approximately seven times larger than the nozzle exit diameter ($L = 7D_j$). The plots were available for a maximum value of $L = 6D_j$; therefore only the A320 and A330 spectra were adjusted ($L = 4D_j$ and $L = 5D_j$, respectively). From the experimental research by Rego et al. it can be expected that for the B777 the low-frequency range is more amplified due to the longer chord length. However, this is only true when jet noise is of the same importance for the B777 as for other aircraft types, which is not the case.

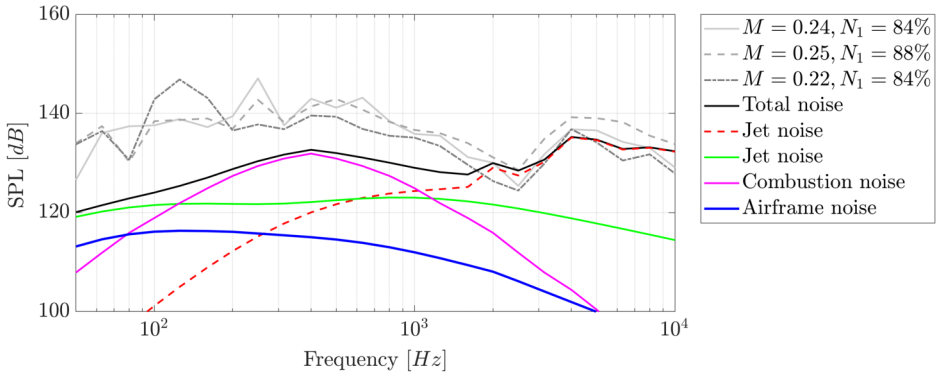

Fig. 22 Comparison of the predicted and measured spectra of the A330 for takeoff.

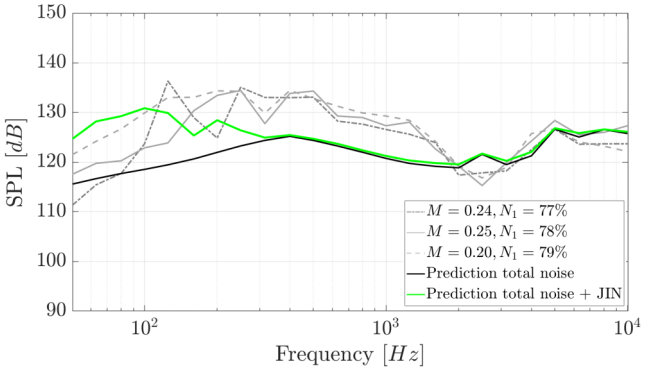

Fig. 23 Experimental and predicted spectra (with and without jet installation noise) of the A320 during takeoff.

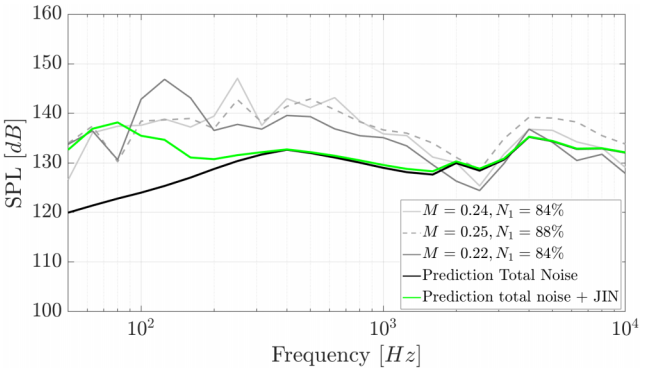

Fig. 24 Experimental and predicted spectra (with and without jet installation noise) of the A330 during takeoff.

Figure 23 shows the measured and predicted (with and without JIN) spectra of the A320 during takeoff. The noise spectrum with JIN shows a better agreement with the experimental data, due to a substantial increase of the SPL at low frequencies up to 400 Hz. Including the jet installation noise also improved the agreement between measured and predicted spectra for the case of the A330, as can be observed in Fig. 24.

These results show that the semi-empirical models can be significantly improved by including the jet installation noise. However, it is important to emphasize that the values of jet installation noise used in this work were not obtained specifically for the geometry and operating conditions of the A320 and A330 aircraft here analyzed. Furthermore, the radial position of the wing with respect to the engine is assumed the same as in Rego's work, which could explain the offset at midfrequencies. Additionally, the values from Rego et al. [4] are based on a flat plate instead of a cambered wing with flaps. Especially the bottom camber of the wing is expected to influence the noise reflection and hence the spectrum.

V. Conclusions

This work analyzed the sensitivity to geometric parameters and operating conditions of semi-empirical noise models typically used to predict aircraft noise. The comparison between flyover measurements and predictions is an exhaustive process due to the level of detail of the input required for the semi-empirical models. The geometric parameters required for the predictions are often not public information, particularly for the engine. In addition, the variation of the operating conditions of the aircraft observed experimentally requires a considerable number of simulations of the engine performance.

The sensitivity analysis showed that the predictions could not reproduce the noise spectrum variability observed experimentally, because the variation range of the operating conditions is not expected to affect the results. Therefore, the average experimental values of the aircraft velocity, altitude, and rotational speed of the fan can be used for the predictions, which significantly decrease the complexity of the comparison.

Engine noise was analyzed for takeoff conditions, whereas airframe noise was studied for landing. The operating conditions and dimensions of the engine and airframe were varied 20% relative to the baseline values. This variation pretends to represent the variability of the operating conditions observed during flyover measurements and approximations of the aircraft geometry.

It was observed that jet noise depends mostly on the aircraft velocity and the rotational speed of the fan, due to the change of the inner and outer jet velocity. Approximating other input parameters is not expected to affect the jet noise spectrum, when within 20% of the real value.

Fan noise, as expected, is influenced by the rotational speed of the fan, but the aircraft altitude and velocity do not play an important role and can be approximated.

Combustion noise also requires an accurate prediction of N_1 due to the N_1 influence on the pressure at the inlet of the combustor. In addition, a wrong estimate of the parameter T_{ref} (which depends on the temperature difference between the exit of the combustor and turbine and pressure at the inlet of the combustor) can result in a significant deviation of the value of combustion noise. Airframe noise showed a significant variation with the aircraft velocity and the number of flap slots.

The comparison between the experimental and predicted spectra for takeoff aircraft (A320 and B777) showed an underprediction of jet noise at low frequencies, which is attributed to jet-installation noise effects, such as reflections on the wing. This effect was less evident for landing aircraft, due to the reduced contribution of the jet to the total noise.

The jet installation noise was added to the predictions based on CAA results available in the literature. Based on these results, the reflection of jet noise is more evident in the low-frequency range. However, according to the experimental spectra of the A320 and A330 aircraft, noise reflection is also expected in the midfrequency region. The reason behind this unexpected result can be a result of the simplification of the wing geometry and the radial wing placing. More work is required in this topic, with dedicated CAA analyses for an aircraft type.

The predicted and experimental spectra for landing aircraft (A320, A330, and B777) have a lower agreement at high frequencies than that observed for takeoff aircraft, indicating an underestimation of the higher harmonics of the fan. The liner dimensions were not available and therefore were approximated based on literature. Consequently, the predicted and experimental spectra of the three aircraft present some differences in the midfrequency region (between 800 and 1600 Hz).

This research work suggests that the semi-empirical noise predictions can be used to compare the noise levels of different aircraft types under different operating conditions but that the models need to be completed with data obtained from experiments or high-fidelity methods for accurate results.

References

[1] Filippone, A., and Harwood, A., "Flyover Noise Measurements and Predictions of Commercial Airplanes," *Journal of Aircraft*, Vol. 53, No. 2, 2016. https://doi.org/10.2514/1.C033370

[2] Bertsch, L., Simons, D., and Snellen, M., "Aircraft Noise: The Major Sources, Modelling Capabilities, and Reduction Possibilities," *1st Joint DLR & TU Delft Aviation Noise Workshop*, Göttingen, Germany, 2015. https://doi.org/10.34912/ac-n0is3

[3] Merino-Martínez, R., Neri, E., Snellen, M., Kennedy, J., Simons, D., and Bennett, G., "Multi-Approach Study of Nose Landing Gear Noise," *Journal of Aircraft*, Vol. 57, No. 3, 2020. https://doi.org/10.2514/1.C035655

[4] Rego, L., Avallone, F., Ragni, D., and Casalino, D., "Jet-Installation Noise and Near-Field Characteristics of Jet-Surface Interaction," *Journal of Fluid Mechanics*, Vol. 895, May 2020. https://doi.org/10.1017/jfm.2020.294

[5] Vieira, A., Snellen, M., and Simons, D., "Assessing the Shielding of Engine Noise by the Wings for Current Aircraft Using Model

Predictions and Measurements," *Journal of the Acoustical Society of America*, Vol. 143, No. 1, 2018, pp. 388–398. https://doi.org/10.1121/1.5020798

[6] Vieira, A., Snellen, M., and Simons, D., "Assessment of Engine Noise Shielding by the Wings of Current Turbofan Aircraft," *24th International Congress on Sound and Vibration*, International Institute of Acoustics and Vibration, 2017.

[7] Synodinos, A., Self, R., and Torija, A., "Framework for Predicting Noise-Power-Distance Curves for Novel Aircraft Designs," *Journal of Aircraft*, Vol. 55, No. 2, 2018. https://doi.org/10.2514/1.C034466

[8] Pietrzko, S., and Bütikofer, R., "FLULA—Swiss Aircraft Noise Prediction Program," *Acoustics 2002—Innovation in Acoustics and Vibration*, Australian Acoustical Soc., 2002, pp. 92–99.

[9] Schäffer, B., Plüss, S., Thomann, G., and Bütikofer, R., "Aircraft Noise Calculations for Relevant Periods of Day Using a Complete Set of Radar Data," *NAG/DAGA proceedings, International Conference on Acoustics Including the 35th German Annual Conference on Acoustics (DAGA)*, Acoustical Society of the Netherlands (NAG) and German Acoustical Society (DEGA), 2009, pp. 1414–1417.

[10] Bertsch, L., Dobrzynski, W., and Guérin, S., "Tool Development for Low-Noise Aircraft Design," *Journal of Aircraft*, Vol. 47, No. 2, 2010. https://doi.org/10.2514/1.43188

[11] Zorumski, W., "Aircraft Noise Prediction Program Theoretical Manual, Part 1," NASA TM 83199, 1982.

[12] Gillian, R., "Aircraft Noise Prediction Program User's Manual," NASA TM 84486, 1982.

[13] Antoine, N., and Kroo, I., "Aircraft Optimization for Minimal Environmental Impact," *Journal of Aircraft*, Vol. 41, No. 4, 2004. https://doi.org/10.2514/1.71

[14] Bertsch, L., Guerin, S., Looye, G., and Pott-Pollenske, M., "The Parametric Aircraft Noise Analysis Module—Status Overview and Recent," *17th AIAA/CEAS Aeroacoustics Conference (32nd AIAA Aeroacoustics Conference)*, AIAA Paper 2011-2855, 2011. https://doi.org/10.2514/6.2011-2855

[15] Bertsch, L., Schäffer, B., and Guerin, S., "Uncertainty Analysis for Parametric Aircraft System Noise Prediction," *Journal of Aircraft*, Vol. 56, No. 2, 2019. https://doi.org/10.2514/1.C034809

[16] Emmerling, J., Kazin, S., and Matta, R., "Core Engine Noise Control Program. Vol 3: Prediction Methods, suppl. 1: Extension of Prediction Methods," FAA FAA-RD-74-125, 1976.

[17] Ho, P., and Doyle, V., "Combustion Noise Prediction Update," *5th AIAA Aeroacoustics Conference*, AIAA Paper 1979-0588, 1979. https://doi.org/10.2514/6.1979-588

[18] *GSP 11 User Manual*, GSP Development Team, Nationaal Lucht- en Ruimtevaartlaboratorium, National Aerospace Lab. (NLR), 2016.

[19] Heidmann, M., "Interim Prediction Method for Fan and Compressor Source Noise," NASA TMX-71763, 1977.

[20] Tyler, J., and Sofrin, T., "Axial Flow Compressor Noise Studies," *SAE Transactions*, Vol. 70, Jan. 1962. https://doi.org/10.4271/620532

[21] Kontos, K., Kraft, R., and Gliebe, P., "Improved NASA ANOPP Noise Prediction Computer Code for Advanced Subsonic Propulsion Systems. Volume 2: Fan Suppression Model Development," NASA CR-202309, 1996.

[22] Stone, J., Krejsa, E., Clark, B., and Berton, J., "Jet Noise Modeling for Suppressed and Unsuppressed Aircraft in Simulated Flight," NASA TM 2009-215524, 2006.

[23] Stone, J., Groesbeck, D., and Zola, C., "An Improved Prediction Method for Noise Generated by Conventional Profile Coaxial Jets," NASA TM 82712 AIAA-81, 1991.

[24] Fink, M., "Airframe Noise Prediction Method, FAA Research," FAA-RD-77-29, 1977.

[25] Fink, M., "Noise Component Method for Airframe Noise," *4th Aeroacoustics Conference*, AIAA Paper 1977-1271, 1977. https://doi.org/10.2514/6.1977-1271

[26] Simons, D., Snellen, M., van Midden, B., Arntzen, M., and Bergmans, D., "Assessment of Noise Level Variations of Aircraft Flyovers Using Acoustic Arrays," *Journal of Aircraft*, Vol. 52, No. 5, 2015. https://doi.org/10.2514/1.C033020

[27] "ICAO Annex 16, Volume I and Equivalent Procedures," International Civil Aviation Organization, 2006, https://www.icao.int/Meetings/EnvironmentalWorkshops/Documents/Noise-Certification-Workshop-2006/Boettcher_3.pdf [retrieved 15 May 2021].

[28] Underbrink, J., "Circularly Symmetric, Zero Redundancy, Planar Array Having Broad Frequency Range Applications," U.S. Patent Number 6,205,224 B1, 2001.

[29] Vieira, A., Snellen, M., and Simons, D., "Experimental Assessment of Sound Quality Metrics for Takeoff and Landing Aircraft," *AIAA Journal*, Vol. 59, 2021, pp. 240–249. https://doi.org/10.2514/1.J059633

[30] Prime, Z., and Doolan, C., "A Comparison of Popular Beamforming Arrays," *Annual Conference of the Australian Acoustical Society 2013, Acoustics 2013: Science, Technology and Amenity*, 2013, pp. 151–157.

[31] Merino-Martinez, R., Snellen, M., and Simons, D., "Functional Beamforming Applied to Imaging of Flyover Noise on Landing Aircraft," *Journal of Aircraft*, Vol. 53, No. 6, 2016, pp. 1830–1843. https://doi.org/10.2514/1.C033691

[32] Schläter, S., and Becker, S., "Determination of Aircraft Engine Speed Based on Acoustic Measurements," *Internoise 2016*, Institute of Noise Control Engineering, 2016, pp. 3858–4854.

[33] Snellen, M., Merino-Martínez, R., and Simons, D., "Assessment of Noise Variability of Landing Aircraft Using Phased Microphone Array," *Journal of Aircraft*, Vol. 54, No. 6, Nov. 2017, pp. 2173–2183. https://doi.org/10.2514/1.C033950

[34] Arntzen, M., "Aircraft Noise Calculation and Synthesis in a Non-Standard Atmosphere," Ph.D. Thesis, Delft Univ. of Technology, Delft, The Netherland, 2014. https://doi.org/10.4233/uuid:c56e213c-82db-423d-a5bd-503554653413

[35] Attenborough, K., "Sound Propagation in the Atmosphere," *Handbook of Acoustics*, Springer, New York, 2014. https://doi.org/10.5860/choice.45-2674

[36] Rego, L., Ragni, D., Avallone, F., Casalino, D., Zamponi, R., and Schram, C., "Jet-Installation Noise Reduction with Flow-Permeable Materials," *Journal of Sound and Vibration*, Vol. 498, April 2020. https://doi.org/10.1016/j.jsv.2021.115959